Thermoelastic and electronic properties of $Bi_{1-x}Sb_x$ and similarly bound materials

H. Köhler, G. Herold, M. Kunkel, and H. Pauly
Physikalisches Institut, Universität Würzburg, 97074 Würzburg, Federal Republic of Germany
(Received 5 May 1993)

The thermoelastic effect (TEE) of perfectly grown $Bi_{1-x}Sb_x$ crystals shows a clear periodic behavior as a function of the composition parameter x with a period of 5.5% for $0 \le x \le 0.19$. Melting and subsequent rapid solidification of the samples causes this phenomenon to disappear, leading to the assumption of superlattice incorporation of the Sb constituents into the bismuth matrix in the first case. Furthermore, since the weakest bonds should dominate the TEE, they have to be correlated with the electronic energy extrema at the L points of the pseudocubic Brillouin zone. Insertion of Sb and Bi atoms in the ratio 1:2 into one of the trigonal layers with a trigonal lattice constant over three double layers leads to a $\frac{1}{3}$ occupation of the superlattice for $x=0.055$ with equidistant hexagonal layers. The assumption of two different sp^3d^2 and p^3d^3 valence hybrids suggests a relation between the superlattice crystal axes and the main axes of the L-band constant-energy surfaces, which also applies to V_2VI_3, IV-VI, IV-VI_2, and similar materials.

I. INTRODUCTION

The electronic properties of bismuth and $Bi_{1-x}Sb_x$ crystals have been the subject of a large variety of experimental techniques and a great number of papers. In particular, experiments in magnetic fields, e.g., cyclotron resonance and magnetoquantum oscillations, have revealed a complex energy-band structure. Numerous energy-band calculations have been performed, yielding nonparabolic $E(\mathbf{k})$ relations for the L-band charge carriers.[1,2] For pure bismuth, the semimetallic properties are deduced from the energy overlap of the T valence band (the constant-energy surface centered at the T point of the pseudocubic Brillouin zone) and the L conduction band (centered at the three L points). Though the experimental results are most significant for pure bismuth, their analysis is often difficult as a consequence of the superposition of contributions from the electrons and holes simultaneously. Therefore, a balanced doping and composition may be advantageous, as demonstrated in a previous paper.[3]

The experiments on the thermoelastic effect (TEE) described in the present paper were performed on neighboring crystal pieces of the same bars grown for the investigation of magnetoquantum oscillations,[3] or equivalently solidified samples with other compositions. The details of the crystal preparation are described in Ref. 3. We realized that the chemical doping of the crystals does not influence the TEE detectably, and samples of comparable doping for different x or several degrees of doping for a fixed Sb content were generally used. We find that the magnitude of the TEE is a distinct, periodic function of the Sb content in the samples, and that the periodicity disappears after melting and subsequent rapid quenching.

II. THEORETICAL BACKGROUND

The essentials of the hydrostatic TEE were described by Swalin,[4] and in a more direct way in Ref. 5 by use of the enthalpy $H=U+pV$ (U denotes the internal energy, p the pressure, and V the volume). For the total differential

$$dH = T\,dS + V\,dp\ , \tag{1}$$

the natural variables p and S (entropy) yield

$$T=(\partial H/\partial S)_p \quad \text{and} \quad V=(\partial H/\partial p)_s\ , \tag{2}$$

and the integrability condition corresponds to

$$(\partial T/\partial p)_S=(\partial V/\partial S)_p=(\partial V/\partial T)_p/(\partial S/\partial T)_p\ . \tag{3}$$

Using the definitions for the isobaric thermal-expansion coefficient $\alpha=(\partial V/\partial T)_p/V$ and the isobaric specific-heat capacity $c_p=T(\partial S/\partial T)_p$, Eq. (3) becomes

$$(\partial T/\partial p)_S=\alpha VT/c_p=\beta\gamma T/\kappa\ , \tag{4}$$

where γ denotes the Grüneisen parameter, β the isothermal compressibility, and $\kappa=c_p/c_V\approx 1$ for a solid. Hence, for $c_p=3R$, the average of T near room temperature and a given volume V, α is related to the reversible temperature variation ΔT on application of a finite stress Δp. In order to eliminate irreversible thermal transport, ΔT has to be determined at the switching time $t=0$ of the stress

$$\lim_{t\to 0}(\Delta T/\Delta p)_S=\Delta T(0)/\Delta p\ . \tag{5}$$

The reversibility was shown because almost the same results for $|\Delta T(0)|$ were obtained both for application and release of stress, within experimental error.

It may be shown[5] that the binding potential φ of a solid for $T=0$ may be developed around the equilibrium distance r_0 as

$$\varphi=\varphi(r_0)+f_h u_n^2/2+f_{\text{anh}}u_n^3/6+O(u_n^4)\ , \tag{6}$$

with $f_h=(\partial^2\varphi/\partial r^2)_{r_0}$ and $f_{\text{anh}}=(\partial^3\varphi/\partial r^3)_{r_0}$, where u_n denotes the displacement of the lattice element n from r_0.

For $T>0$, in a linear approximation for the augmented equilibrium distance $r^*=(1+\varepsilon)r_0$, the equivalent expansion for φ finally yields[5]

$$\alpha=-k_B f_{\text{anh}}/(2r_0 f_h^2) \tag{7}$$

in a first-order expansion up to u_n^3 in Eq. (6). Since f_{anh}/f_h is high for weak bonds, in an inhomogeneously bound crystal the weakest bonds should contribute the maximum effect to the TEE. Therefore, this phenomenon allows us to observe the variation of the weakest bonds as a function of change in the significant crystal parameters.

III. EXPERIMENTAL DETAILS

The $Bi_{1-x}Sb_x$ crystals with space group D_{3d}^5 ($0\le x\le 0.19$) were grown by thorough mixing of the constituents, rapid solidification, and subsequent twofold zone melting in opposite directions, in order to compensate the segregation of the components, with about 0.5 mm/h velocity. The samples were cut from the central parts of the bars by an acid string saw (Honeywell etch: H_2O, HCl, and CrO_3); the composition there by repeated investigation was shown to be equal to that of the mechanically mixed and rapidly solidified ingot. The sample shape corresponds to an approximate half cylinder of about 1 cm^3 volume. Hydrostatic stress was applied in a stainless-steel vessel of about two orders of magnitude greater volume, filled with water at about 4 °C, the anomaly point of the thermal-expansion coefficient of H_2O. In this arrangement, the influence of the TEE of the stress-transmitting medium could be neglected or, for a small contribution in case of $T\neq 4$ °C, be included in the calculation.[5]

Numerical treatment of the nonstationary thermal transport allows us to optimize the effect by the choice of the contact points (spot welding) for the thermocouple wires (Ni-NiCr; about 40 μV/K, where the sample forms one of the two "solder contacts" of the thermocouple and the other is kept at constant temperature.[5] In this case, $\Delta T(t)$ shows an almost exact exponential decay over several seconds, which allows a reliable extrapolation of $\Delta T(0)$. A possible small systematic error cancels out in comparison of results for different stress values, applied and released, and comparison of the data for different samples as a function of the composition. The reversibility condition was fulfilled by extrapolation towards $t=0$ (time of stress switching), and possible contact effects could be eliminated by repeated measurements with different thermocouple contacts.

The thermovoltages U_{th} ranged up to the order of 4 μV for stresses $|\Delta p|$ up to 250 bar, corresponding to values of $|\Delta T(0)|$ of about 100 mK at maximum. U_{th} was measured by a galvanometer amplifier (Amplispot-Sefram and Nanomat-Burster) and data processing was performed by analog-to-digital transformation and PC implementation.

IV. RESULTS

A typical $U_{\text{th}}(t)$ curve is shown in Fig. 1, where the stress-switching interval is much smaller than 1 s. The

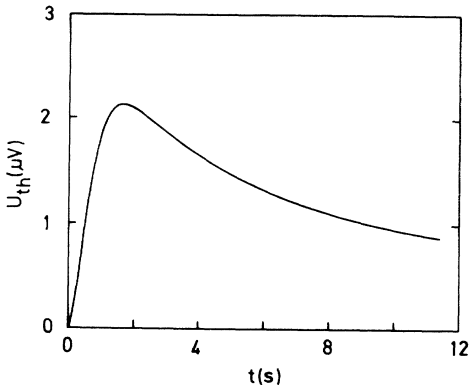

FIG. 1. Thermovoltage U_{th} (Ni-NiCr) as a function of time for a typical sample after application of a stress Δp at $t=0$. The exponential decay for $t>2$ s originates from the thermal conduction into the surrounding medium. For discussion, see text.

increase below 2 s after stress switching at $t=0$ is caused by the relaxation times of the amplifier circuit. This range is not used for the evaluation. In Fig. 2(a), and (b) $|\Delta T(t)|$ is shown on a semilogarithmic scale, the least-squares-fit straight lines confirming the exponential decay for $t>2$ s, for different stress values (a) applied and (b)

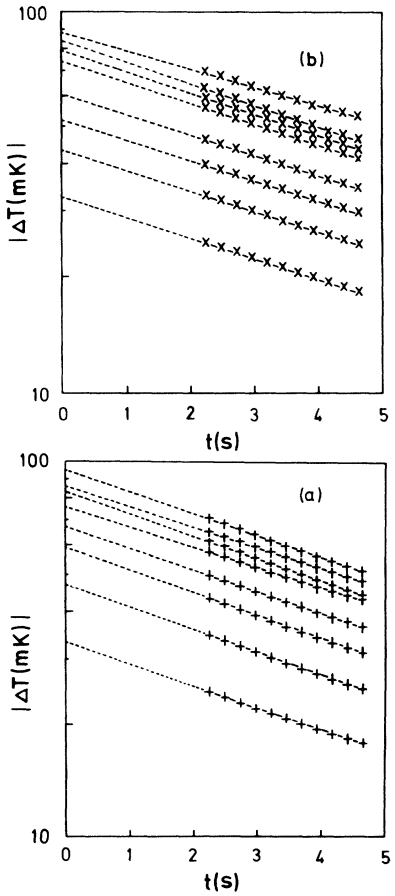

FIG. 2. Semilogarithmic plot of $|\Delta T(t)|$ for (a) application and (b) release at different values for $|\Delta p|$, increasing from the bottom to the top. The linear dependences for $t>2$ s are extrapolated (dashed lines) towards $t=0$, yielding the reversible temperature shift $|\Delta T(0)|$.

released. Without including experimental errors, for equivalent nonstationary thermal conductivities into the surrounding medium, the inclination of the straight lines in Fig. 2 is determined by the so-called temperature conductivity.

In Fig. 3 the extrapolated $|\Delta T(0)|$ values for different $|\Delta p|$ of a typical sample are plotted for $\Delta p > 0$ (+) and $\Delta p < 0$ (×). The fitted curves are parabolas, indicating that the isobaric thermal-expansion coefficient is not constant in the stress range investigated. In Eq. (7), the equilibrium distance r_0 decreases as a function of $\Delta p > 0$, but simultaneously f_h increases, so that $r_0 f_h^2$ increases and α decreases linearly. This is demonstrated in Fig. 4 for the binding potential $\varphi(r)$ for $T=0$ with and without a linear stress-induced potential φ_p, where $\varphi_{\text{tot}}(r)=\varphi(r)+\varphi_p$ possesses a higher harmonic content around its shifted minimum compared to $\varphi(r)$. This means that, in lowest order, $\Delta T(0)/\Delta p$ contains a linear and a squared term, which was taken into account in the fit of Fig. 3. The thermoelastic effect, in the calculation, is considered as the linear term for $\Delta p \to 0$.

The TEE results as a function of the composition are shown in Fig. 5 for the slowly solidified samples. Clear maxima and minima are distinguished with a periodicity of $\Delta x = 5.5$ at. %. The sawtooth curve is drawn—lacking a known analytic dependence—as a guide to the eye. It is obvious that the decay of the TEE with increasing x is steeper than the ascent. The scatter of the data, besides a small difference between application and release of stress, may be caused by systematic errors, such as some deviation in the composition x or an uncertainty in the fabrication of the thermocouple contacts by spot welding of the Ni-NiCr wires. These errors should be small, but may hardly be quantified reliably.

Another surprising effect is the disappearance of the periodic structure in Fig. 5 after melting and rapid solidification of the samples (with an increase of the growth velocity by a factor of about 10^5), since, under hydrostatic pressure, the change in the outer shape of the samples should not be of importance. In Fig. 6 any periodic effect in the TEE as a function of x has vanished; the slightly upward-sloping straight line was obtained by a least-squares fit. The average values of $\Delta T(0)/\Delta p$ in Fig. 6 correspond to the minima in Fig. 5. It appears

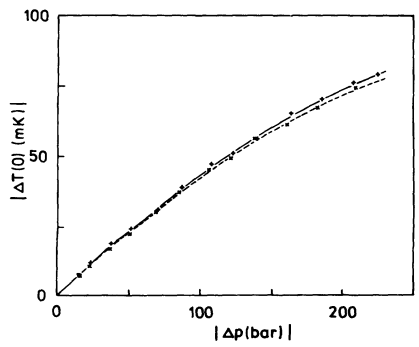

FIG. 3. Extrapolated temperature shifts $|\Delta T(0)|$ for different stress values $|\Delta p|$, for application (+) and release (×) of the stress. For discussion, see text.

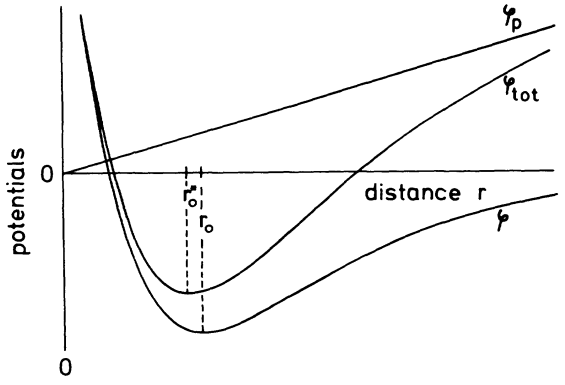

FIG. 4. Schematic binding potentials φ, φ_p, and $\varphi_{\text{tot}}=\varphi+\varphi_p$ as a function of distance r. φ_{tot}, around r_0^*, possesses a higher harmonic content than φ around r_0.

that disorder in the samples makes the TEE periodicity in x vanish.

V. DISCUSSION

The results of the preceding section indicate the obvious presence of weaker and stronger bonds in the $Bi_{1-x}Sb_x$ crystals; this is also supported by the formation of double layers with different internal and external lattice spacings. The peculiarity in the periodicity of the TEE as a function of the composition ($\Delta x = 5.5$ at. %) can be related to the electronic properties, i.e., the zero-gap state for the L energy bands and the crossover of the different valence-band edges. In Fig. 7 the shift of the band edges as a function of x is plotted, where the gap energies are given by Golin[6] in a linear approximation:

$$E_{T_{45}^-} - E_{L_s} = 38.5 - 500x \text{ meV} , \tag{8a}$$

$$E_{L_s} - E_{L_a} = 15.3 - 270x \text{ meV} . \tag{8b}$$

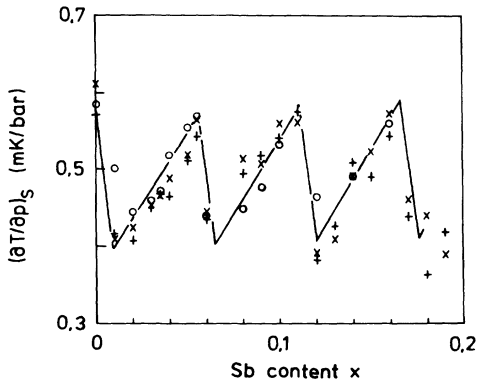

FIG. 5. Linear thermoelastic effect $(\partial T/\partial p)_s$ for $\Delta p \to 0$ as a function of the composition parameter x for different $Bi_{1-x}Sb_x$ crystals ($0 \le x \le 0.19$). (×) denotes application and (+) release of stress. (○) is the average of both for a different experiment (thermocouple) and the same or a different sample.

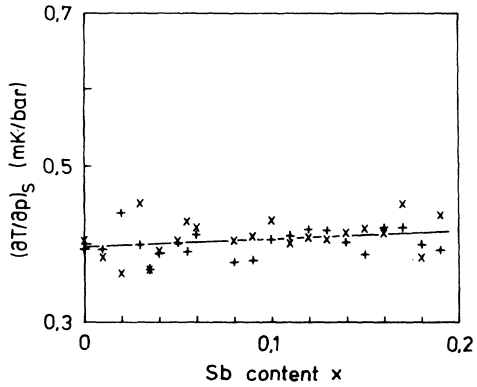

FIG. 6. Linear TEE $(\partial T/\partial p)_s$ after melting and subsequent rapid solidification of the samples. As in Fig. 5 (×) denotes application and (+) release of the stress. For discussion, see text.

Equation (8b) yields $E_{L_s}=E_{L_a}$ for $x_L=0.056$, and Eq. (8a) $E_{T_{45}^-}=E_{L_s}$ for $x_{L_sT}=0.077$. However, in contrast to the gap energies for $x=0$, the composition coefficients do not seem to be very accurate.[6] Substitution of 275.4 for 270 meV yields $x_L=0.0\bar{5}$, and of 500 by 346 meV corresponds to $x_{L_sT}=0.\bar{1}=2x_L$. The crossover of the L_s and H_v valence-band edges is usually assumed to be at $x_{L_sH}=3x_L=0.1\bar{6}$ (Fig. 7). The intersections of the L_a conduction-band edge with the T_v and H_v valence-band edges at about 8.7 and 22 at. % mark the limits of semimetallic and semiconductive behavior.

The fact that the TEE shows a maximum also for pure bismuth indicates that the effects observed cannot exclusively be attributed to an Sb superstructure in a Bi matrix for x_L, x_{L_sT}, and x_{L_sH} in a perfectly grown crystal. The weak bonds have to exist also for pure bismuth crystals. Therefore, we propose two kinds of valence hybrids: sp^3d^2 and p^3d^3, the latter, more excited, for the superlattice constituents, the sites of which are occupied preferably by the Sb atoms for low x values. The two kinds of sites are in one each of every double layer. For $x_L=0.0\bar{5}$,

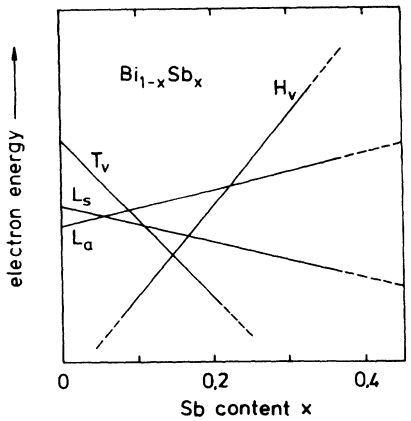

FIG. 7. Schematic shift of the electronic energy-band edges of $Bi_{1-x}Sb_x$ crystals as a function of the composition on the Bi-rich side (small x values).

the antimony atoms form an orthorhombic net with a $\sqrt{3}$ times higher lattice constant in the trigonal planes in every third double layer; in the same layers, the Bi atoms for $x_{L_sT}=0.\bar{1}$ exhibit the p^3d^3 bonds, where the Sb atoms form a honeycomb matrix and sp^3d^2 hybrids. At 16.7 at. % Sb content, a 1:5 intercalation of antimony layers in Bi is reached. The alternation between Bi and Sb superlattice p^3d^3 valencies in every third double layer at $x=0$ or $0.\bar{1}$, and $0.0\bar{5}$ or $0.1\bar{6}$, respectively, is indicated by the sawtooth variation in Fig. 5.

This means that the six p^3d^3 valencies are completely filled, with a roughly two times greater binding length compared with the sp^3d^2 hybrids. Since the average number of valence electrons is five, the sp^3d^2 hybrids, with the same configuration as the p^3d^3 valencies, cannot be occupied completely. It is easily seen that, in the layers of constituents with both valencies, the sp^3d^2 bonds are connected to six neighbors, three each in two adjacent layers with exclusively sp^3d^2-bound Bi atoms. There, vice versa, only four neighbors exist for the sp^3d^2 bonds, so that—in average over all bonds—only five electrons per constituent are needed, where all existing covalent bonds between neighbors are occupied by exactly two electrons at any time. The higher excited p^3d^3 hybrids possess roughly twice as large a binding length. The different strength of binding for the sp^3d^2 and p^3d^3 hybrids explains the formation of the double layers. There is no need for resonance valence bonds, and a consistent model for the crystal binding (not including some ionic contribution) in the five-electron system is obtained by this proposal.

The relation between the thermoelastic and electronic properties is easily intelligible. For $x=0$, p^3d^3 bonds are formed in a pure Bi sublattice. The smallest admixture of Sb causes disorder in this subsystem, which makes the TEE drop rapidly. This disorder in the trigonal planes vanishes towards $x=0.0\bar{5}$, and starts again for $x>0.\bar{5}$, when the Bi atoms enter the p^3d^3 hybrids preferentially up to $x=0.\bar{1}$. This sequence is repeated for $x>0.\bar{1}$ up to $x=0.1\bar{6}$ for Sb, and possibly even further, when the next two layers of mixed valencies are occupied by Sb constituents. For $x=0.0\bar{5}$, in the trigonal direction, for the p^3d^3 bonds there exists a superstructure with a periodicity of two compared to the basic lattice, and an additional Sb superstructure with period 3 for the p^3d^3 layers. This makes the energies for the symmetric and antisymmetric wave functions become equivalent, leading to a zero gap between L_s and L_a states. At $x=0.\bar{1}$, according to the regular cubic p^3d^3 structure of the Bi atoms only, the valence-band energies of the T and L points obviously cannot be distinguished, so that a crossover of E_T and E_{L_s} occurs, if E_T also is associated with the p^3d^3 bonds. This sequence is repeated for $x=0.1\bar{6}$, when the same number of Sb atoms form p^3d^3 valencies, leading to maxima at the L points and the T point (or the adjacent H for $x\rightarrow 1$) of the pseudocubic Brillouin zone.

A further peculiarity is the tilt angle of 5.8° of the constant-energy-surface main axes in the mirror planes of $Bi_{1-x}Sb_x$ for the L bands. Consideration of the double-layer structure (with layer distances $d_{\text{intra}}=d_a=3.10$ Å

and $d_{\text{inter}}=d_r=3.47$ Å for pure bismuth) and the further Sb superlattice periodicity over three double layers for the tilt angle Θ relative to the crystal axes yields

$$\Theta=\arctan\{(\tfrac{1}{6})[1+(d_r-d_a)/(d_r+d_a)]/\sqrt{3}\}$$
$$=5.80^\circ, \quad (9)$$

instead of 30° for a cubic lattice ($d_a=d_r$) without an Sb superstructure.

It is simple to apply this idea to similarly bound materials with, on average, the same number of valence electrons, e.g., the IV-VI semiconductors, such as PbTe, PbSe, GeTe, SnTe, etc. They form perfect NaCl-type structures, so that, for $d_a=d_r$ and no superstructure, by substitution the tilt angle Θ [Eq. (9)] becomes 30°, as observed for PbTe and PbSe. The valence electrons are equivalently distributed between sp^3d^2 and p^3d^3 hybrids, the latter developing around every third group-IV atom in any of these (111) layers, forming a hexagonal distribution with 3 times higher site distance. Six group-IV neighbors are bound in the second-nearest atomic layers. The rest of the constituents develop partially filled sp^3d^2 hybrids with six and four occupied bonds, respectively. Hence, a minimum of electronic charge has to be transferred between the group-IV and -VI layers (the electronic charge centers of the p^3d^3 valencies are in the group-VI layers). The opposite, p^3d^3 hybrids developing around the group-VI constituents, may also occur, associated with lattice defects and nonstoichiometry, which would explain n- and p-type conduction, for instance, for lead salts.

We have also investigated the TEE on SnTe samples, grown by the Bridgman method, with a varying nonstoichiometry (tin defect; p-type conduction). In Fig. 8 the results are shown as a function of the hole concentration obtained from the Hall effect up to $B=7.4$ T and $T=4.2$ K, which should be a measure for the tin defect concentration. The TEE first decreases with the concentration, and then increases above 1.7×10^{21} cm^{-3} (the result at 2×10^{21} cm^{-3} is the average of repeated measurements on the same sample with different thermocouple contacts, since no other samples were available). The

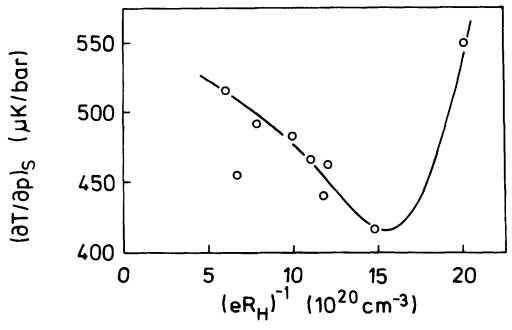

FIG. 8. Thermoelastic effect $(\partial T/\partial p)_s$ (average of application and release of the stress) of nonstoichiometric SnTe as a function of the low-temperature Hall hole concentration $(eR_H)^{-1}$. The curve is drawn as a guide to the eye. For discussion, see text.

minimum at 1.7×10^{21} cm^{-3} for a 1:1 correspondence of the hole concentration and the tin defects per volume would correspond to missing p^3d^3 tin constituents in every third layer $\frac{1}{9}$, where $\frac{1}{9}$ denotes tin defects per volume. This sheds light on the connection of nonstoichiometry and the electronic p^3d^3 configuration and corresponds to the Sb substitution in $Bi_{1-x}Sb_x$, where the respective sites in trigonal projection coincide, too. The zero-gap composition in $Pb_{1-x}Sn_xTe$ (Pb substitution by Sn in the p^3d^3 states) is reached at $x=\frac{1}{3}$,[7] i.e., in any lead (111) layer every third Pb atom is substituted by Sn, exhibiting the p^3d^3 hybrids.

Similar results on Bi_2Te_3 for the TEE as a function of nonstoichiometry were obtained and published earlier,[8] by using the fact that the Te defect leads to p conductivity. It was concluded that the central $Te^{(2)}$ layers (periodic $\cdots$-$Te^{(1)}$-Bi-$Te^{(2)}$-Bi-$Te^{(1)}$-$\cdots$ stacking in trigonal direction) perpendicular to the trigonal axis (space group D_{3d}^5 as for Bi) contain the tellurium defects, which should be—according to the above discussion—associated with the p^3d^3 sites. If the saturation (or even minimization) of the TEE at about 2×10^{19} cm^{-3} (stable Hall concentration) and a 1:1 correspondence to the $Te^{(2)}$ defects are assumed, a $1:243=(\frac{1}{3})\times(\frac{1}{81})$ dilution should occur, which is likely possible as a result of the considerable $Te^{(1)}$-$Te^{(1)}$ intercalation between and in ($Te^{(2)}$) the Bi double layers (in comparison to Bi). Again, a disintegration into separate sp^3d^2 and p^3d^3 hybrids allows saturation of all necessary covalent bonds by two electrons without the postulation of resonance bonds. The $Te^{(2)}$ layers should contain the p^3d^3 sites in a 1:3 dilution, with a corresponding higher binding length over the fivefold layers to the six equivalent neighbors. The sp^3d^2 bonds connect a varying number of covalently bound neighbors (Te and Bi, respectively), leading to saturated bonds between all neighbors, too. Equivalent arguments apply to Bi_2Se_3 and Sb_2Te_3.

If one considers Bi_2Te_3 as a system of hexagonal Bi double layers [$d_a=4.06$ Å; $d_r=6.11$ Å; Eq. (9)] with one internal and two external intercalated Te layers, the tilt angle of the main axes of the constant-energy surfaces becomes (omitting the factor $\frac{1}{6}$ as a result of the missing superstructure, as in the case of bismuth),

$$\Theta_{Bi_2Te_3}=\arctan\{[1+(d_r-d_a)/(d_r+d_a)]/\sqrt{3}\}$$
$$=34.7^\circ, \quad (10)$$

instead of 30° for the cubic case. Such results were evaluated earlier.[9,10]

The considerable dilution of $Te^{(2)}$ defects in the trigonal planes for the stable configuration (grown from a stoichiometric melt, 1:27, compared to $Bi_{1-x}Sb_x$ with $x=\frac{1}{18}$), e.g., in a hexagonal configuration, yields almost the same defect-superlattice constant parallel and normal to the trigonal axis, whereby the Coulomb energy is minimized.

Furthermore, the IV-VI_2 compounds (e.g., $SnSe_2$) may also be placed into this kind of solid with a periodic layer ordering of $\cdots$-VI-IV-VI-$\cdots$ along the trigonal axis. The p^3d^3 hybrids in 1:3 dilution should occur in the

group-IV layers, which allows the development of completely filled covalent bonds with six (p^3d^3) and on average five (sp^3d^2) neighbors.

VI. CONCLUSION

It is shown above that investigation of thermoelastic properties as a function of constituent substitution or defect concentration is a powerful tool to understand covalent binding and the electronic properties of perfectly grown crystals. Here, the contribution of mixed valencies (sp^3d^2 and p^3d^3 hybrids) provides perfect saturation of all bonds by two electrons and allows a relation of the bonding to the electronic energy bands of $Bi_{1-x}Sb_x$ and a discussion of the crossover of the band edges. Thereby, an understanding of semimetallic behavior and nonstoichiometry is attained, and this may be generalized to a large variety of different crystal systems.

The discussion above does not claim completeness with respect to the development of such mixed valencies. Certainly other examples may be found and, perhaps, the model proposed is the basic physical reason for nonstoichiometry on the whole. This investigation is left to future work. The most interesting effect should be the formation of superstructures in a large number of solids, partially of lower dimensionality (equivalent to modern thin-film preparational techniques), which were not perceived over previous decades.

[1]S. Golin, Phys. Rev. **166**, 643 (1968).
[2]J. W. McClure and K. H. Choi, Solid State Commun. **21**, 1015 (1977).
[3]H. Köhler, H. J. Leister, and A. Gensler, Phys. Rev. B **41**, 7724 (1990).
[4]R. Swalin, *Thermodynamics of Solids* (Wiley, New York, 1972), p. 33.
[5]W. Baier and H. Köhler, J. Phys. Condens. Matter **3**, 307 (1991).
[6]S. Golin, Phys. Rev. **176**, 830 (1968).
[7]L. Esaki and P. T. Stiles, Phys. Rev. Lett. **16**, 1108 (1966).
[8]P. Dato and H. Köhler, J. Phys. C **17**, 3711 (1984).
[9]H. Köhler, Phys. Status Solidi B **73**, 95 (1976).
[10]H. Köhler, Phys. Status Solidi B **74**, 591 (1976).